

Stresses Due to Tangential and Normal Loads on an Elastic Solid With Application to Some Contact Stress Problems

By J. O. SMITH¹ AND CHANG KENG LIU,² URBANA, ILL.

The results of two-dimensional approach using real variable method to Hertz's problem of contact of elastic bodies are presented. Both normal and tangential loads are assumed to be distributed in Hertzian fashion over the area of contact. The magnitude of the intensity of the tangential load is assumed to be linearly proportional to that of the normal load when sliding motion of the body is impending. The stresses in the elastic body due to the application of these loads on its boundary are presented in closed form for both plane-stress and plane-strain cases. A numerical value of $f = 1/3$ is assumed for the linear proportionality (coefficient of friction) between the tangential and normal loads in order that the distribution of stresses may be illustrated. The significance of the stress distribution, across the contact area and in the body, is also discussed. It is shown that when the combination of loads considered in the paper are applied at the contact area of bodies in contact the maximum shearing stress may be at the surface instead of beneath the surface. For example, for plane strain, if the coefficient of friction is $f = 1/3$, the maximum shearing stress is at the surface and is 43 per cent larger than the maximum shearing stress, which would be below the surface, that occurs when the normal force acts alone. The effect of range of normal stress and of shearing stress on the plane of maximum shear and on the plane of maximum octahedral shear on failure by progressive fracture (fatigue) is discussed.

INTRODUCTION

THE problem of the contact of elastic bodies under normal loading was first investigated by H. Hertz (1)³ in 1881. He computed and verified with experiment the load distribution over the contact area, and solved for the stresses in the body in terms of a Newtonian potential function. S. Fuchs (2) in 1913, performed a laborious arithmetical integration to obtain the stresses. Eight years later, W. B. Morton and L. J. Close (3), using zonal harmonics, calculated the stresses in a half space on which a spherical ball is pressed by a normal load. At about

the same time (as Morton and Close) Coker and Ahmed (4) studied analytically and experimentally a plane-stress problem where a portion of the boundary of a half plane is loaded with normal pressure. In 1930, H. R. Thomas and V. A. Hoersch (5) transformed the Hertzian solution for the stresses on the axis of symmetry into standard elliptical integrals and discovered that the shearing stress on the axis of symmetry is maximum at some distance underneath the center of the contact area. Their computation of the stresses is checked by agreement with experiment. Independently, Belajef (6) calculated the stresses at any point in the half space by the use of elliptical co-ordinates. His solution gives similar results on the axis of symmetry to those obtained by Thomas and Hoersch. L. Foepl (7), in 1936, also obtained a similar solution for the problem of a cylinder and a spherical ball pressed on a flat plate, and verified the results by a photo-elastic experiment.

The effect on the stresses due to the presence of a tangential load, however, was not taken into consideration by investigators until 1939, when G. Lundberg (8) developed a general theory of elastic contact between two semi-infinite bodies. In his theory, he introduced three potential functions which correspond to three components of the load along three axes of a Cartesian coordinate. The components of the load tangent to the contact area presumably are regarded as frictional forces between the contact surfaces. He made no attempt to find the stresses caused by the frictional forces in addition to the normal load.

R. D. Mindlin (9), in 1949, investigated the distribution of tangential load across the area of contact when one elastic body slides over the other. He found that the stress on the bounding curve of the contact area due to the tangential load is infinite and consequently a state of impending slipping prevails. Corresponding to this condition the intensity of tangential force at a point in the contact area cannot usually exceed the product of the coefficient of friction between the sliding surfaces and the normal pressure at the same point. In this paper, a value of $1/3$ is used for the coefficient of friction, in order to show the stress distributions due to the tangential load superimposed on the normal load acting over the same area of contact.

In December, 1949, not long after the authors completed their solution of this problem, H. Poritsky (10) presented a solution of the same problem (he uses a coefficient of friction of 0.3) by means of an Airy's function. The results, independently obtained by two different methods, agree. In this paper the authors have extended the results of the solution to include an interpretation of the significance of these stresses in causing failure by inelastic yielding and by fatigue.

EQUATIONS FOR STRESSES

Plane-Stress Problem: Concentrated Forces—Normal or Tangential. From elasticity theory, the stresses in a half plane due to a concentrated force p , acting either normally or tangentially to its boundary as shown in Figs. 1(a) and (b), respectively, are

¹ Professor of Theoretical and Applied Mechanics, University of Illinois. Mem. ASME.

² Formerly, Associate of Theoretical and Applied Mechanics, University of Illinois. Jun. ASME.

³ Numbers in parentheses refer to the Bibliography at the end of the paper.

Contributed by the Applied Mechanics Division and presented at the Annual Meeting, New York, N. Y., November 30-December 5, 1952, of THE AMERICAN SOCIETY OF MECHANICAL ENGINEERS.

Discussion of this paper should be addressed to the Secretary, ASME, 29 West 39th Street, New York, N. Y., and will be accepted until July 10, 1953, for publication at a later date. Discussion received after closing date will be returned.

NOTE: Statements and opinions advanced in papers are to be understood as individual expressions of their authors and not those of the Society. Manuscript received by ASME Applied Mechanics Division, April 21, 1952. Paper No. 52-A-13.

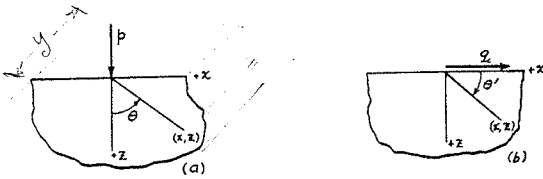


FIG. 1 CONCENTRATED NORMAL LOAD AND TANGENTIAL LOAD ON BOUNDARY

$$\left. \begin{aligned} \sigma_x &= -\frac{2p}{\pi z} \cos^2 \theta \sin^2 \theta \\ \sigma_z &= -\frac{2p}{\pi z} \cos^4 \theta \\ \tau_{xz} &= -\frac{2p}{\pi z} \sin \theta \cos^3 \theta \end{aligned} \right\} \dots \dots \dots [1]$$

$$\left. \begin{aligned} \sigma_x &= -\frac{2q}{\pi z} \cos^3 \theta' \sin \theta' \\ \sigma_z &= -\frac{2q}{\pi z} \cos \theta' \sin^3 \theta' \\ \tau_{xz} &= -\frac{2q}{\pi z} \sin^2 \theta' \cos^2 \theta' \end{aligned} \right\} \dots \dots \dots [2]$$

in which

$$\theta = \text{arc cos } \frac{z}{\sqrt{z^2 + x^2}}, \text{ and } \theta' = \text{arc cos } \frac{x}{\sqrt{x^2 + z^2}}$$

Stresses Due to Distributed Normal Forces.⁴ If the normal forces as just discussed are distributed along a portion of the boundary of the half plane, as shown in Fig. 2, the stresses in the

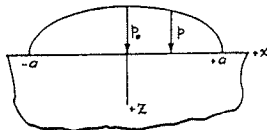


FIG. 2 ELLIPTICAL DISTRIBUTION OF NORMAL LOAD ON BOUNDARY

half plane are

$$\left. \begin{aligned} \sigma_{xn} &= -\frac{p_0}{\pi} z \left[\frac{a^2 + 2x^2 + 2z^2}{a} \bar{\Psi} - \frac{2\pi}{a} - 3x\psi \right] \\ \sigma_{zn} &= -\frac{p_0 z}{\pi} [a\bar{\Psi} - x\psi] \\ \tau_{xzn} &= -\frac{p_0}{\pi} z^2 \psi \end{aligned} \right\} \dots \dots [3]$$

⁴ If the normal load per unit of length in the y -direction applied on the boundary is P , then $p_0 = \frac{2P}{\pi a}$, Fig. 2. The value of a , the half width of the contact area, may be found for two cylindrical cylinders whose longitudinal axes are parallel, that are in contact along a line, from the equation $a = \sqrt{\frac{2P\Delta}{\pi}}$ in which

$$\Delta = \frac{1}{2} \left(\frac{1}{R_1} + \frac{1}{R_2} \right) \left[\frac{1 - \mu_1^2}{E_1} + \frac{1 - \mu_2^2}{E_2} \right]$$

The symbols R_1 , μ_1 , and E_1 represent the radius, Poisson's ratio, and modulus of elasticity, respectively, for one cylinder, and R_2 , μ_2 , and E_2 have similar meaning for the second cylinder.

in which

$$\left. \begin{aligned} \psi &= \frac{\pi}{K_1} \frac{1 - \sqrt{\frac{K_2}{K_1}}}{\sqrt{\frac{K_2}{K_1}} \sqrt{2\sqrt{\frac{K_2}{K_1}} + \left(\frac{K_1 + K_2 - 4a^2}{K_1} \right)}} \\ \bar{\Psi} &= \frac{\pi}{K_1} \frac{1 + \sqrt{\frac{K_2}{K_1}}}{\sqrt{\frac{K_2}{K_1}} \sqrt{2\sqrt{\frac{K_2}{K_1}} + \left(\frac{K_1 + K_2 - 4a^2}{K_1} \right)}} \end{aligned} \right\} \dots [4]$$

$$\begin{aligned} K_1 &= (a + x)^2 + z^2 \\ K_2 &= (a - x)^2 + z^2 \end{aligned}$$

Stresses Due to Distributed Tangential Forces. In a similar manner, the stresses in a half plane due to a tangential force dis-

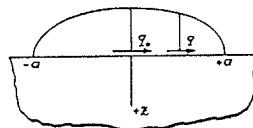


FIG. 3 (left) ELLIPTICAL DISTRIBUTION OF TANGENTIAL LOAD ON BOUNDARY

tributed along a portion of its boundary as shown by the ordinates to the ellipse in Fig. 3 are given by the following equations

$$\left. \begin{aligned} \sigma_{xt} &= -\frac{q_0}{\pi} \left[(2x^2 - 2a^2 - 3z^2)\psi + 2\pi \frac{x}{a} + 2(a^2 - x^2 - z^2) \frac{x}{a} \bar{\Psi} \right] \\ \sigma_{zt} &= -\frac{q_0}{\pi} z^2 \psi \\ \tau_{xzt} &= -\frac{q_0}{\pi} \left[(a^2 + 2x^2 + 2z^2) \frac{z}{a} \bar{\Psi} - 2\pi \frac{z}{a} - 3xz\psi \right] \end{aligned} \right\} \dots [5]$$

in which $\bar{\Psi}$ and ψ denote the same quantities as expressed by Equations [4].

An examination of Equations [3] and [5] reveals that, except for a constant multiplier, σ_{xt} and τ_{xzn} have identical form, and so do τ_{xzt} and σ_{zn} .

In order to facilitate the plotting of the stresses against x while z is taken as a parameter, the values of ψ and $\bar{\Psi}$ are first computed from Equations [4]. Table 1 shows the values of ψ and $\bar{\Psi}$ for various values of x and z where z is taken as 0.125a, 0.25a, 0.375a, 0.50a, 0.75a, 1.00a, 1.50a, and 2.00a. It is seen that $\bar{\Psi}$ is symmetrical to x , whereas ψ is symmetrical to the origin.

Stresses on Boundary Due to Distributed Normal and Tangential Forces. Special consideration is given to the computation of the stresses in the area of contact. They can be shown to be expressed, respectively, by the following equations:

(A) For distributed tangential load on boundary

$$i \sigma_{xt} = \begin{cases} -2q_0 \left[\frac{x}{a} - \sqrt{\frac{x^2}{a^2} - 1} \right] & \text{for } x \geq a \\ -2q_0 \left[\frac{x}{a} + \sqrt{\frac{x^2}{a^2} - 1} \right] & \text{for } x \leq -a \\ -2q_0 \frac{x}{a} & \text{for } |x| \leq a \end{cases} \dots [6]$$

⁵ The derivation of Equations [4] can be found in reference (11).

TABLE 1 VALUES OF ψ AND $\bar{\Psi}$

$\frac{z}{a}$	$z = 0.125a$		$z = 0.25a$		$z = 0.375a$		$z = 0.50a$	
	ψ	$\bar{\Psi}$	ψ	$\bar{\Psi}$	ψ	$\bar{\Psi}$	ψ	$\bar{\Psi}$
0	0	0	0	0	0	0	0	0
0.025	±0.017175	+0.068769	±0.017059	+0.068520	±0.016869	+0.068109	±0.016609	+0.067542
0.05	±0.043995	+0.132244	±0.043408	+0.131239	±0.042456	+0.129603	±0.041181	+0.127390
0.075	±0.189648	+0.381269	±0.181679	+0.370867	±0.169666	+0.355007	±0.155094	+0.335404
0.1	±0.681510	+1.034918	±0.596645	+0.933123	±0.494131	+0.818711	±0.397638	+0.702863
0.125	±10.281792	+11.649858	±3.286846	+4.224414	±1.618003	+2.349094	±0.946560	+1.552699
0.15	±8.125376	+11.204954	±3.200000	+4.800000	±1.644113	+2.750869	±0.962013	+1.814951
0.175	±4.434819	+9.053184	±1.983798	+4.290146	±1.128147	+2.659019	±0.703155	+1.840884
0.2	±3.136568	+8.515818	±1.435473	+4.103299	±0.837865	+2.591848	±0.533935	+1.823685
0.225	±2.011807	+8.181206	±0.932308	+3.976819	±0.552732	+2.539731	±0.357433	+1.805773
0.25	±0.984018	+7.997064	±0.458916	+3.904208	±0.274341	+2.507644	±0.178875	+1.793268
0.275	0	+7.938238	0	+3.880572	0	+2.496877	0	+1.788855
0.3	±0.015900	+0.065979	±0.014985	+0.063919	±0.012783	+0.058734	±0.010456	+0.052826
0.325	±0.037866	+0.121520	±0.033907	+0.114263	±0.025644	+0.098004	±0.018508	+0.082202
0.35	±0.123658	+0.291460	±0.094958	+0.248603	±0.053975	+0.179423	±0.030949	+0.132013
0.375	±0.251632	+0.517119	±0.161253	+0.390254	±0.071873	+0.242207	±0.035479	+0.163798
0.4	±0.415822	+0.865845	±0.217287	+0.568865	±0.076980	+0.307921	±0.033323	+0.194222
0.425	±0.409649	+0.991404	±0.206280	+0.638105	±0.068606	+0.334686	±0.028377	+0.206565
0.45	±0.315303	+1.048121	±0.159598	+0.680775	±0.051689	+0.354278	±0.020750	+0.215385
0.475	±0.245772	+1.059185	±0.125429	+0.693299	±0.040439	+0.361111	±0.016079	+0.219237
0.5	±0.167802	+1.064253	±0.086294	+0.701305	±0.027778	+0.365955	±0.010973	+0.221656
0.525	±0.084988	+1.066196	±0.043935	+0.705709	±0.014139	+0.368842	±0.005564	+0.223118
0.55	0	+1.066667	0	+0.707107	0	+0.369800	0	+0.223607

NOTE: Entries in this table are to be multiplied by π/a^2 , where a is the half length of the loading region on the boundary.

ii $\tau_{xz} = \begin{cases} -q_0 \sqrt{1 - \frac{x^2}{a^2}} & \text{for } |x| \leq a \\ 0 & \text{for } x \geq a, \text{ and } x \leq -a \end{cases} \dots [7]$

iii $\sigma_{zt} = 0$ for all points on boundary.... [8]

(B) For distributed normal load on boundary

i $\sigma_{zn} = \begin{cases} -p_0 \sqrt{1 - \frac{x^2}{a^2}} & \text{for } |x| \leq a \\ 0 & \text{for } x \geq a, \text{ and } x \leq -a \end{cases} \dots [9]$

ii $\sigma_{zn} = \begin{cases} -p_0 \sqrt{1 - \frac{x^2}{a^2}} & \text{for } |x| \leq a \\ 0 & \text{for } x \geq a, \text{ and } x \leq -a \end{cases} \dots [10]$

iii $\tau_{zxn} = 0$ for all points on boundary.... [11]

A complete picture of stresses in the half plane is plotted from Equations [3], [5], and [6] through [11]. They are shown in Figs. 4 to 7.

In reality, any presence of tangential load must be associated with that of normal load. Hence the stresses from Equations [3] and [5] (plotted in Figs. 4 to 7), should be superimposed upon each other, provided the quantities p_0 and q_0 are related by some law. According to Mindlin (9), $q_0 = fp_0$, where f denotes the coefficient of friction of the surfaces of contact; f can vary in a wide range in accordance with the surface conditions of the bodies in contact. For the purpose of illustration, f is assumed to be equal to $1/3$. Thus the stresses due to combined application of distributed normal and tangential loads, as expressed in terms of p_0 when $f = 1/3$, become

$\sigma_z^* = -\frac{p_0}{\pi} \left\{ (a^2 + 2x^2 + xz^2) \frac{z}{a} \bar{\Psi} - 2\pi \frac{z}{a} - 3xz\psi + \frac{1}{3} \left[(2x^2 - 2a^2 - 3z^2)\psi + 2\pi \frac{x}{a} + 2(a^2 - x^2 - z^2) \frac{x}{a} \bar{\Psi} \right] \right\} \dots [12]$

$\sigma_x^* = -\frac{p_0}{\pi} z \left[a\bar{\Psi} - x\psi + \frac{z}{3} \psi \right]$ (11)

$\tau_{xz}^* = -\frac{p_0}{\pi} \left\{ x^2 \psi + \frac{1}{3} \left[(a^2 + 2x^2 + 2z^2) \frac{z}{a} \bar{\Psi} - 2\pi \frac{z}{a} - 3xz\psi \right] \right\} \dots [12]$ (Continued)

in which z is always greater than zero, i.e., for the points in the half plane. For the points on the boundary the stresses become

$\sigma_{z/z=0}^* = \begin{cases} -\frac{2}{3} p_0 \left[\frac{x}{a} - \sqrt{\frac{x^2}{a^2} - 1} \right] & \text{for } x \geq a \\ -p_0 \left[\sqrt{1 - \frac{x^2}{a^2}} + \frac{2x}{3a} \right] & \text{for } |x| \leq a \\ -\frac{2}{3} p_0 \left[\frac{x}{a} + \sqrt{\frac{x^2}{a^2} - 1} \right] & \text{for } x \leq -a \end{cases} \dots [12a]$

$\sigma_{z/z=0}^* = \begin{cases} -p_0 \sqrt{1 - \frac{x^2}{a^2}} & \text{for } |x| \leq a \\ 0 & \text{for } x \geq a \text{ and } x \leq -a \end{cases}$

$\tau_{xz/z=0}^* = \begin{cases} -\frac{1}{3} p_0 \sqrt{1 - \frac{x^2}{a^2}} & \text{for } |x| \leq a \\ 0 & \text{for } x \geq a \text{ and } x \leq -a \end{cases}$

PLANE-STRAIN PROBLEM

In the preceding section the stresses have been found for a state of plane stress. For a state of plane strain two principal stresses are the same as for plane stress, but the third principal stress σ_y , is not zero as in the case for plane stress. The stress σ_y in the y -direction (perpendicular to the xz -plane) for the case of plane strain (contact of long cylinders) due to combined application of distributed tangential and normal loads is

$\sigma_y^* = \nu(\sigma_x^* + \sigma_z^*) \dots [13]$

where ν is the Poisson's ratio of the material. When Equations [12] are substituted into Equation [13], the following is obtained

$\sigma_y^* = -\frac{2\nu}{\pi} p_0 \left\{ \left[(a^2 + x^2 + z^2) \frac{z}{a} \bar{\Psi} - \frac{\pi z}{a} - 2xz\psi \right] + \frac{1}{3} \left[(x^2 - a^2 - z^2)\psi + \frac{\pi x}{a} + (a^2 - x^2 - z^2) \frac{x}{a} \bar{\Psi} \right] \right\} \dots [14]$

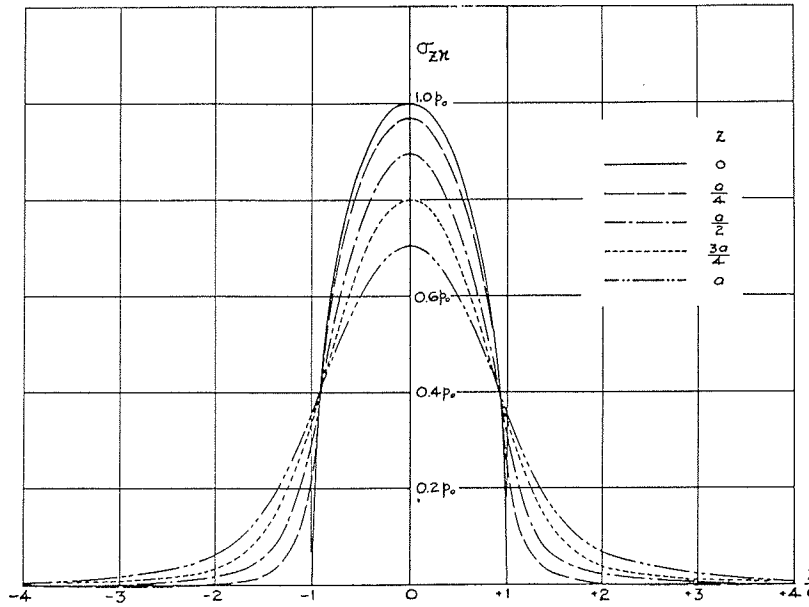


FIG. 4 CURVES SHOWING VALUES OF STRESS σ_{zn} FOR VARIOUS VALUES OF x , AT SURFACE AND AT VARIOUS DEPTHS BELOW SURFACE (See Fig. 2, for loading.)

Consequently, on the boundary, the stress in y -direction is expressed by the following equations corresponding to their respective regions

$$\sigma_{y/z=0} = \begin{cases} -\nu p_0 \frac{2}{3} \left[\frac{x}{a} - \sqrt{\frac{x^2}{a^2} - 1} \right] & \text{for } x \geq a \\ -\nu p_0 \left[2 \sqrt{1 - \frac{x^2}{a^2}} + \frac{2}{3} \frac{x}{a} \right] & \text{for } |x| \leq a \\ -\nu p_0 \frac{2}{3} \left[\frac{x}{a} + \sqrt{\frac{x^2}{a^2} - 1} \right] & \text{for } x \leq -a \end{cases} \dots [15]$$

In later calculations, ν is assumed to be equal to $1/4$.

MAXIMUM STRESSES AND THEIR SIGNIFICANCE

Introduction. The results of the preceding sections may be used to solve certain problems involving contact stresses, for example, for computing the stresses in two cylindrical rollers of the same material, whose longitudinal axes are parallel, that are pressed against each other, Fig. 8(a), while one or both cylinders are rotated about a longitudinal axis causing a sliding friction force between the rollers, as shown in Fig. 8(b). The normal and tangential loads are distributed over the area of contact as shown in Fig. 8(c). In this section the results of computations of the stresses in the cylinders in this example will be given, but before this is done, it should be noted that the significance of the maximum values of stress cannot be determined apart from a knowledge of what action constitutes failure of the roller.

While it is not possible here to describe all types of failure of such rollers it can be said that failure generally occurs in one of two main types. The term failure is used to mean any action which will destroy the load-carrying capacity. Failure from contact stresses starts as a localized inelastic deformation (yielding or distortion) and by fracture, especially fracture by progressive spreading of a crack (fatigue). Usually it is assumed that the inelastic deformation type of failure is associated with the maximum shearing stress or with the maximum octahedral

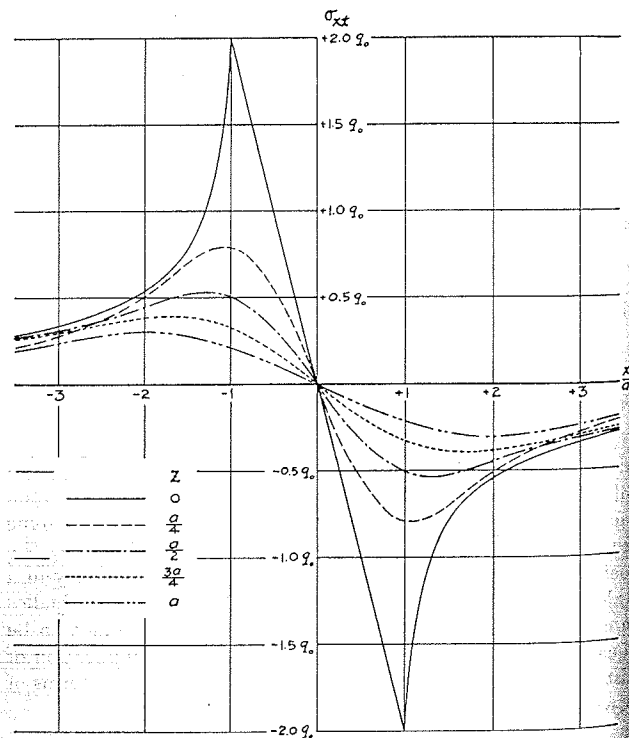


FIG. 5 CURVES SHOWING VALUES OF STRESS σ_{xt} FOR VARIOUS VALUES OF x , AT SURFACE AND AT VARIOUS DEPTHS BELOW SURFACE (See Fig. 3, for loading.)

shearing stress. The maximum shearing stress is given by the equation

$$\tau_{max} = \frac{1}{2} (\sigma_1 - \sigma_3) \dots [16]$$

in which σ_1 and σ_3 are the maximum and minimum values of the principal stresses at the point. The maximum octahedral shearing stress is given by the equation

in which
mediate
The s
applicati
fracture
evidence
surface
stress is
face the
to the s
known
means t
direction
positive

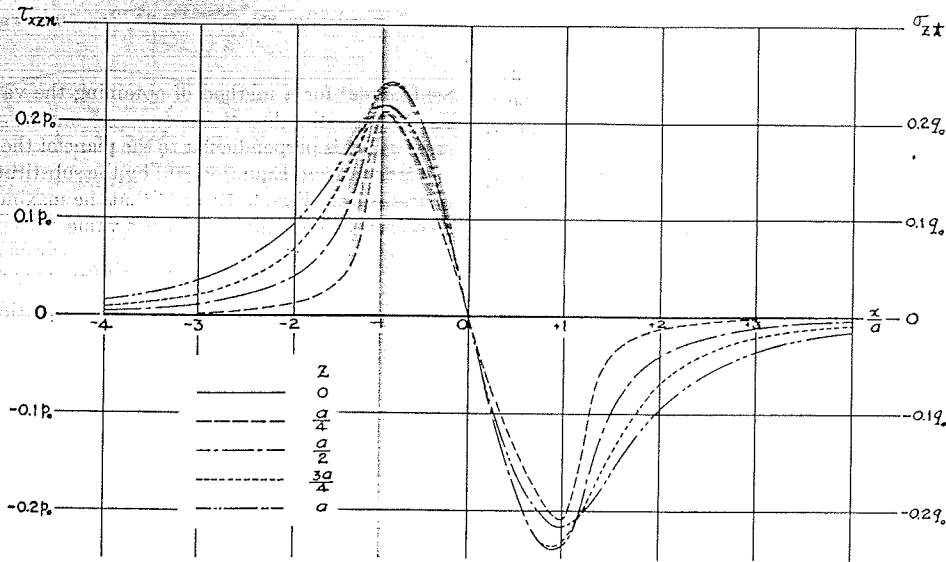


FIG. 6 CURVES SHOWING VALUES OF STRESSES τ_{xzn} , σ_{xz} FOR VARIOUS VALUES OF x , AT SURFACE AND AT VARIOUS DEPTHS BELOW SURFACE (See Figs 1 and 2 respectively, for loading.)

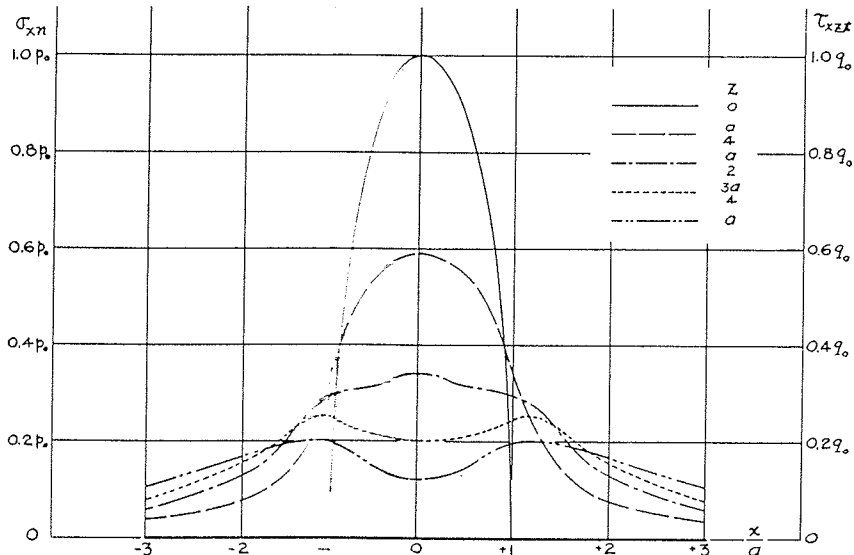


FIG. 7 CURVES SHOWING VALUES OF STRESSES σ_{xzn} , τ_{xzt} FOR VARIOUS VALUES OF x , AT SURFACE AND AT VARIOUS DEPTHS BELOW SURFACE (See Figs 1 and 2 respectively, for loading.)

$$\tau_{G \max} = \frac{1}{3} \sqrt{(\sigma_1 - \sigma_2)^2 + (\sigma_2 - \sigma_3)^2 + (\sigma_3 - \sigma_1)^2}$$

in which σ_1 and σ_2 are defined as before and σ_3 is the third (intermediate value) principal stress.

The second type of failure is associated with many repeated applications of the loads and is characterized by a fatigue fracture that starts as a localized crack with very little visual evidence of inelastic deformation. The crack starts either at the surface or underneath the surface and grows progressively as the stress is repeated until some of the metal breaks out of the surface thereby causing pitting, shelling, or other damaging effects to the surface which constitutes failure. In the type of failure known as fatigue we must know the "range" of stress. This means that we must determine for the roller the magnitude, direction (line of action through point) and sense, that is whether positive or negative, of the stress at a given point on a given plane

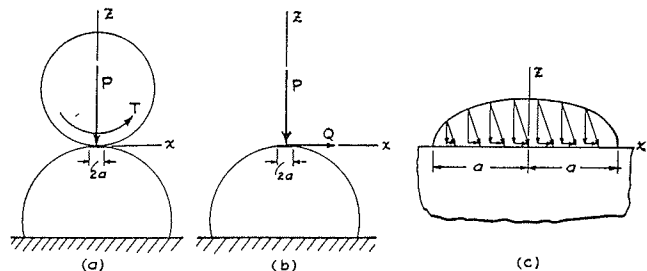


FIG. 8 NORMAL AND TANGENTIAL CONTACT LOADS FOR TWO ROLLERS IN CONTACT

throughout one cycle of application and release of the load. This will be done later in this paper.

In this section of the paper the values of σ_1 , σ_2 , and σ_3 are given for a sufficient number of points in the cross sections of the

25

rollers near the contact area so that the maximum value of τ_{max} and $\tau_{G max}$ may be determined from Equations [16] and [17].

Maximum Stresses. By making use of Equations [12] [12a], [13], [14], and [15], the stresses σ_x^* , σ_y^* , and τ_{xz}^* have been found at points whose x and z -coordinates are given in Table 1. By making use of Mohr's circle the three principal stresses, σ_1^* , σ_2^* , and σ_3^* were determined at each point described in Table 1. From these results contour lines that represent constant values of principal stress, σ_1^* , σ_2^* , and σ_3^* are plotted in Figs. 9, 10, and 11. It is found that at the point A ($z = 0, x = +0.3a$) in Fig. 9, 10, or 11, the maximum values of the three principal stresses occur. These values at the point A are

$$\sigma_1 \max^* = -1.39p_0, \sigma_2 \max^* = -0.72p_0, \text{ and } \sigma_3 \max^* = -0.53p_0 \quad \dots \dots \dots [18]$$

See footnote⁴ for a method of obtaining the values of p_0 and a . Fig. 12 shows the directions of $\sigma_1 \max^*$ and $\sigma_2 \max^*$. The third stress $\sigma_3 \max^*$ is perpendicular to the plane of the other two.

It is found from Equation [16] by the substitution of the values of stresses from Figs. 9, 10, or 11 that the maximum value of τ_{max} also occurs at the point A and has a value

$$\tau_{max} = 0.43 p_0 \dots \dots \dots [19]$$

In a similar manner by making use of Equation [17] it is found

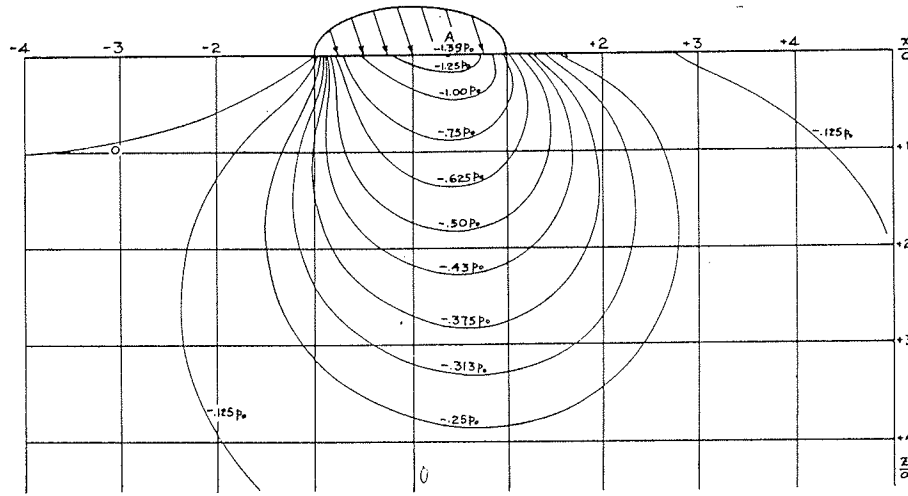


FIG. 9 CONTOURS FOR ONE OF TWO PRINCIPAL STRESSES LYING IN xz -PLANE

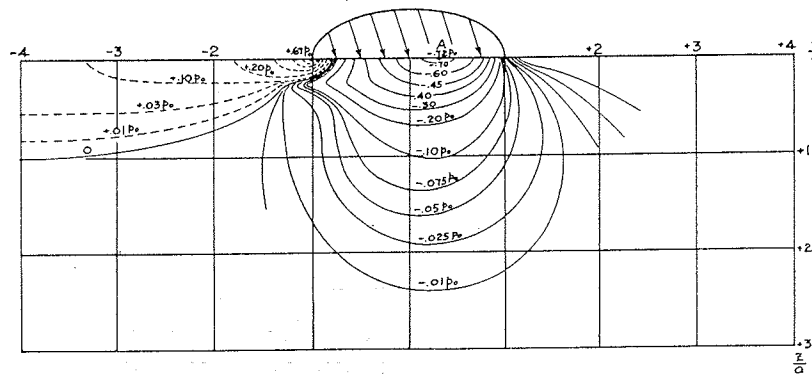


FIG. 10 CONTOURS FOR ONE OF TWO PRINCIPAL STRESSES LYING IN xz -PLANE

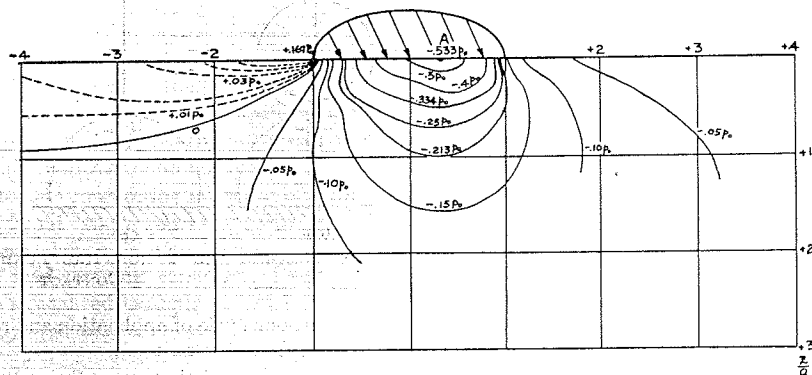


FIG. 11 CONTOURS FOR PRINCIPAL STRESS WHICH ACTS IN Y -DIRECTION

that has

It friction Equ

and tance force maximum by 4 37 p ing from gatic that surf the

Rang point of the plied mov load from zero point the p chan of str

In fixed are g point direc press each given the p stress notec zz-pl fact i in me tion c

6 R

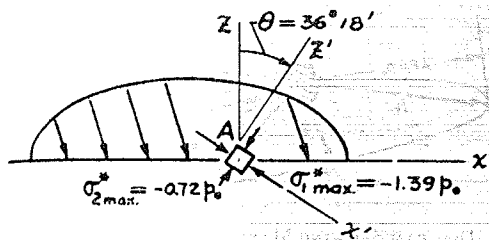


FIG. 12 LOCATION OF MAXIMUM PRINCIPAL STRESSES

that the maximum value of τ_{Gmax} also occurs at the point A and has the value

$$\tau_{Gmax} = 0.37 p_0 \dots \dots \dots [20]$$

It should be noted that if the normal forces act alone, that is, the friction coefficient is assumed to be zero, the stresses as given in Equations [18], [19], and [20] would be, respectively,

$$\sigma_{1max} = -p_0, \sigma_{2max} = -p_0, \sigma_{3max} = -0.5 p_0 \dots \dots [21]$$

$$\tau_{max} = 0.30 p_0 \dots \dots \dots [22]$$

$$\tau_{Gmax} = 0.27 p_0 \dots \dots \dots [23]$$

and these values of τ_{max} and τ_{Gmax} occur⁶ on the z-axis at a distance $z = 0.78a$ underneath the surface. Therefore the tangential force caused by the coefficient of friction of $1/3$ increases the maximum principal stress 39 per cent, the maximum shearing stress by 43 per cent, and the maximum octahedral shearing stress by 37 per cent. Furthermore, the location of these maximum shearing stresses is changed by the addition of the tangential force from beneath the surface to the point A in the surface. Investigation shows that when the coefficient of friction becomes greater than $f = 1/3$, the maximum shearing stress occurs at a point in the surface, but when f is less than $1/3$, this stress is underneath the surface.

Range of Stress for One Load Cycle. In order to determine the range of stress it is necessary to compute the stresses at a given point for several positions of the loads relative to the location of the given point. To state the idea differently, the loads applied to the rollers are assumed to remain constant while the movement of the roller surfaces changes the location at which the loads are applied. At a point located a relatively large distance from the loads the stresses due to these loads are approximately zero. As the loads move nearer to the point the stresses at the point increase. Moreover, as the loads begin to pass over the point the magnitude, line of action, and sense of the stresses change. From a study of these changes in the stresses the range of stress is established.

In Figs. (a) through (i) of Table 2, the point O represents a fixed point in the surface of one of the rollers (the dimensions a are greatly magnified) as the load approaches and passes over the point O. The figures in the second column show the magnitude, direction, and sense (sense here means whether tensile or compressive stress) of the three principal stresses at the point O for each position of the load. In Table 2 the symbol σ_1^* is always given to the principal stress having the largest magnitude, σ_3^* to the principal stress of least magnitude and σ_2^* to the principal stress whose magnitude is intermediate. From Table 2 it is noted that the directions of the two principal stresses that lie in the xz -plane rotate through 90 deg during each load cycle. This fact makes the range of stress more difficult to determine because in most members that are subjected to repeated loads the direction of each of the principal stresses remains fixed during the load

TABLE 2 TABLE SHOWING CHANGES IN MAGNITUDE, SENSE AND DIRECTION OF PRINCIPAL STRESSES AT A FIXED POINT O IN SURFACE, AS LOAD MOVES PAST IT

POSITION OF LOAD RELATIVE TO A FIXED POINT O.	DIRECTION, SENSE AND MAGNITUDE OF PRINCIPAL STRESSES AT FIXED POINT O.
(a)	$\sigma_1^* = 0$ $\sigma_2^* = 0$; $\sigma_3^* = 0$
(b)	$\sigma_1^* = 0$ $\sigma_2^* = -0.67 p_0$; $\sigma_3^* = -0.17 p_0$
(c)	$\sigma_1^* = -0.69 p_0$ $\sigma_2^* = -1.35 p_0$; $\sigma_3^* = -0.51 p_0$
(d)	$\sigma_1^* = -0.72 p_0$ $\sigma_2^* = -1.39 p_0$; $\sigma_3^* = -0.53 p_0$
(e)	$\sigma_1^* = -0.67 p_0$ $\sigma_2^* = -1.33 p_0$; $\sigma_3^* = -0.50 p_0$
(f)	$\sigma_1^* = -1.04 p_0$; $\sigma_2^* = -0.37 p_0$ $\sigma_3^* = -0.36 p_0$
(g)	$\sigma_1^* = -0.61 p_0$; $\sigma_2^* = -0.14 p_0$ $\sigma_3^* = 0.05 p_0$
(h)	$\sigma_1^* = 0.67 p_0$; $\sigma_2^* = -0.17 p_0$ $\sigma_3^* = 0$
(i)	$\sigma_1^* = 0$ $\sigma_2^* = 0$; $\sigma_3^* = 0$

cycle so that only the magnitude and sense of the stress changes. Therefore, in order to make use in this paper of the methods usually employed in describing the effect of range of stress (14), the changes in the stress on a fixed plane through a point O in the surface of the roller will be considered. Three different fixed planes are selected here for this purpose, as discussed in the following paragraphs.

Range of Normal Stress σ_x^* . From the first of Equations [12a] the values of σ_x^* have been computed at points on the surface for various values of x relative to one position of the load. The results are plotted in Fig. 13 in which the ordinates represent values of σ_x^* at each value of x . If the load in Fig. 13 is allowed to move along the surface, then the stress σ_x^* at a fixed point O will have in turn each of the values shown in Fig. 13. Fig. 13 shows that the stress σ_x^* changes from a maximum compression of $-1.20 p_0$ to a maximum tension of $+0.67 p_0$, or, that is, a maximum range of stress of $1.87 p_0$. The stress σ_x^* has been chosen here because it has a greater change in magnitude than the normal stress on any other fixed plane through a fixed point on the surface or underneath the surface. Two important facts about this range of stress should be noted: (a) When this range of normal stress is compared with the range that occurs when there

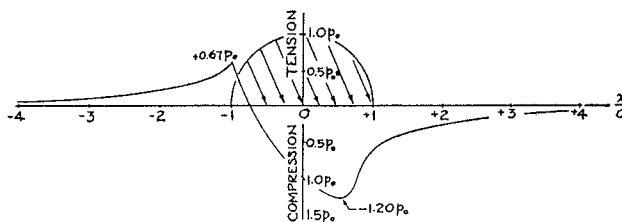


FIG. 13 RANGE OF VALUES OF σ_x^* AT A POINT O (FIXED) AS LOAD MOVES PAST POINT

⁶ Reference (5), p. 29.

27

is no friction force, which is from zero to $-1.0 p_0$ in compression, it is noted that there is an 87 per cent increase in magnitude (coefficient of friction $1/3$). (b) There is a change in the sense of the stress from tension to compression; that is, there is some reversal of stress, a fact that is of considerable importance in explaining how a progressive crack starts and propagates when the stresses are predominantly in compression.

Range of Shearing Stress on Plane of Maximum Shear. The magnitude and direction of the shearing stress on the plane of the maximum shearing stress (plane bisecting angle between σ_1^* and σ_3^* in Fig. d, Table 2) have been computed at the point O for each position of the load as shown in Table 2. In Fig. 14 the vectors

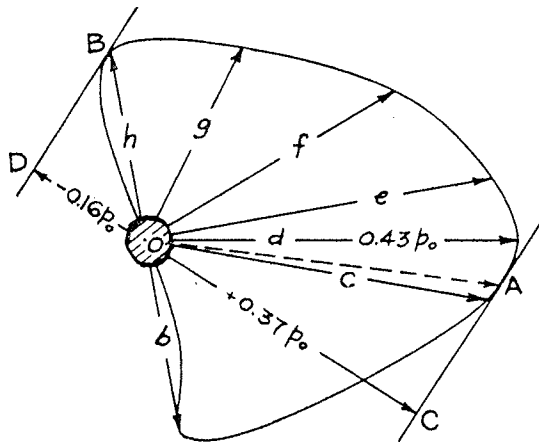


FIG. 14 DIAGRAM SHOWING MANNER IN WHICH MAGNITUDE, SENSE, AND DIRECTION OF SHEARING STRESS VARY ON PLANE OF MAXIMUM SHEAR
($f = 1/3, \mu = 1/4, E = 30,000,000$ psi.)

through the point O marked b, c, and so on through h, respectively, represent these values of the stress. A smooth curve O-A-B is drawn and a vector from O to this curve represents the shearing stress on this particular plane through O for some position of the load. The magnitude of the maximum shearing stress on this plane, therefore, varies from zero to $0.43 p_0$. However, it is seen from Fig. 14 that the changes in direction of the shearing stress are such that along certain lines in the plane there is a change in sense, that is, a reversal of the shearing stress. For example, the vectors marked b and h represent equal and opposite shearing stresses, that is, a complete reversal of stress, each being equal to $0.23 p_0$ or a total range of $0.46 p_0$. But the line C-O-D, where DO is a component of the stress OB and OC is a component of the stress OA, represents the largest range of the shearing stress along all lines that can be drawn in this plane through O. The vectors $OD = -0.16 p_0$ and $OC = +0.37 p_0$ give a total range of $0.53 p_0$ which is 23 per cent greater than the range from zero to $0.43 p_0$ along the vector d in Fig. 14. Furthermore, a comparison of this range of stress of $0.53 p_0$ with the maximum shearing stress⁷ of $0.30 p_0$ when the coefficient of friction is assumed to be zero (Equation [22]) shows an increase of 77 per cent in range of shearing stress due to the addition of the tangential force caused by a friction coefficient of $1/3$.

Range of Shearing Stress on Plane of Maximum Octahedral Shearing Stress. It will now be shown that on the plane of maximum octahedral shearing stress a greater range of shearing stress occurs than that on the plane of maximum shear. In Fig. 15

⁷ E. I. Radzimovsky in reference (13) has shown that when the coefficient of friction is zero the maximum range of shearing stress occurs at a point below the surface on a plane parallel to the x and y-axes, Fig. 8, and this range of stress is from $-0.25 p_0$ to $+0.25 p_0$.

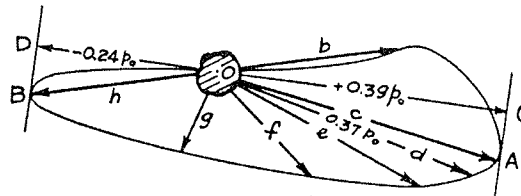


FIG. 15 DIAGRAM SHOWING MANNER IN WHICH MAGNITUDE, SENSE, AND DIRECTION OF SHEARING STRESS VARY ON PLANE OF MAXIMUM OCTAHEDRAL SHEARING STRESS
($f = 1/3, \mu = 1/4, E = 30,000,000$ psi.)

the vectors marked b, c, d, and so on, respectively, represent the shearing stresses on a plane making equal angles with σ_1^* , σ_2^* , and σ_3^* in Fig. d of Table 2, for the corresponding positions of the load in Table 2 and the smooth curve O-A-B is drawn so that any vector from O to the curve represents the shearing stress in this plane through O for some position of the load. The line C-O-D, as was the case in Fig. 14, represents the direction in this plane along which occurs the greatest range of shearing stress. This range consists of $OD = -0.24 p_0$ and $OC = +0.39 p_0$ or a total range of $0.63 p_0$ which is 61 per cent greater than the range⁸ of $0.39 p_0$. The range of shearing stress on the octahedral plane is from zero to $0.27 p_0$ when the coefficient of friction is assumed to be zero (Equation [23]). Thus by comparing $0.63 p_0$ with $0.27 p_0$ it is noted that the tangential force caused by a coefficient of friction of $1/3$ produces an increase of 122 per cent in range of shearing stress.

SIGNIFICANCE OF CONTACT STRESS IN SHELLING FAILURES OF RAILROAD RAILS

Many examples involving the stresses described in the foregoing sections could be given to illustrate the relationship of these stresses with failure, such as pitting failures, bearing races, gear teeth, rolls for rolling steel or other metals, and the like. One such example, namely, the wheel of a locomotive rolling on the rail of a railroad, is chosen for showing the relation of contact stresses with failure of the rail.

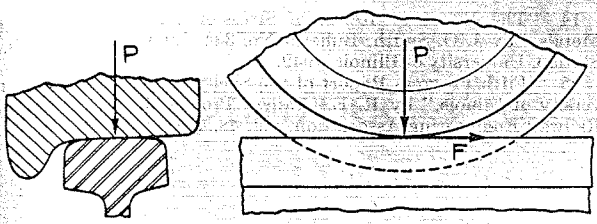
In Fig. 16 are shown the forces of a locomotive wheel on rails of straight and curved railway. The force P is due to the weight of the locomotive, F is a frictional force that, on straight rail, is due to the driving or braking forces applied through the wheel. For a rail on curved track F also includes frictional forces caused by wheel slippage because the wheels are rigidly attached to the axle. The force T is the thrust on the outside rail of a curve due to the centrifugal forces on the train. Both of the forces P and F that occur on curved rail, Fig. 16(b), therefore may be considerably larger than on straight rail, Fig. 16(a).

It might be expected from the foregoing analysis of the forces on the wheels and railway rails that rail failures are more severe on curved rail, where contact stresses due to both normal or tangential forces occur, than on straight rail. Reports contained in the Proceedings of the American Railway Association show that this is the case. R. E. Cramer (15) has described several types of shelly failures of railway rails that frequently occur on curved rail, usually in the outside rail on the curve. Most of these failures are of a progressive fracture type. First phase of the failure is characterized by inelastic strains in the surface layer on top of the rail head and on the rail-head edge in contact with the wheel flange, Fig. 16(b). These inelastic strains probably are caused by the high shearing

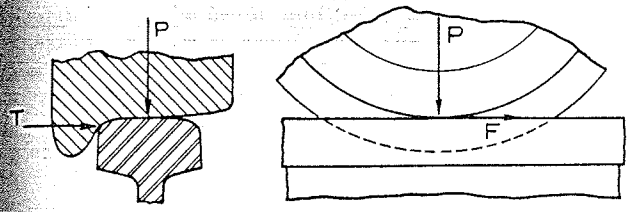
⁸ The reason for omitting the use of distortion energy, which is usually found in discussions of fatigue failure, is shown by these facts. Distortion energy is a scalar quantity that is proportional to the square of the magnitude of the maximum octahedral shearing stress. Hence the range of distortion energy will not have increased corresponding to those shown in Figs. 14 and 15.

(a)
(b)
stress
forces
combi
rail he
(or bo
these
The
portar
materi
of high
Rail
failure
wheel
weight
ing tor

1
1895;
2
mit ein
p. 1282
3
by W.
vol. 43,
4
Ahmed
vol. 1,
5
by H. I
ment. S
6
Belajef.
Contact
ASME,
7
Stoffes
auf den
October
8
berg, F
10, Sep



(a) FORCES ON RAILWAY RAIL FROM LOCOMOTIVE WHEEL ON STRAIGHT RAIL.



(b) FORCES ON RAILWAY RAIL FROM LOCOMOTIVE WHEEL ON CURVED RAIL.

FIG. 16 CONTACT FORCES ON RAILWAY RAIL

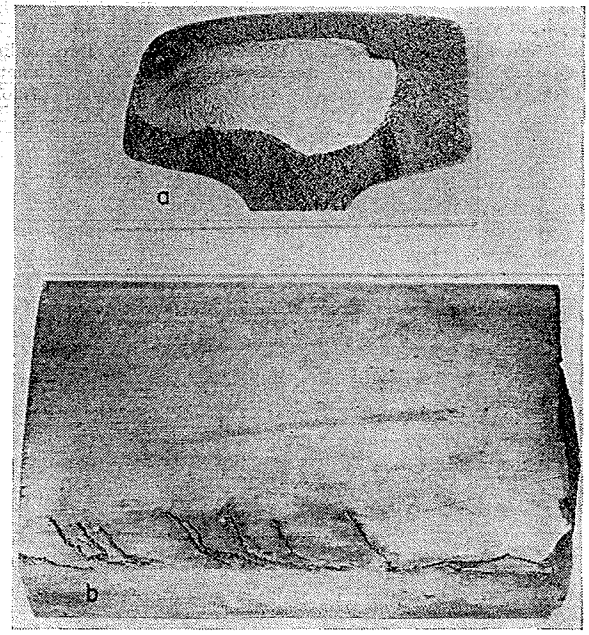


FIG. 17 FATIGUE FAILURE OF RAIL HEAD DUE TO COMBINATION OF NORMAL AND TANGENTIAL LOADING

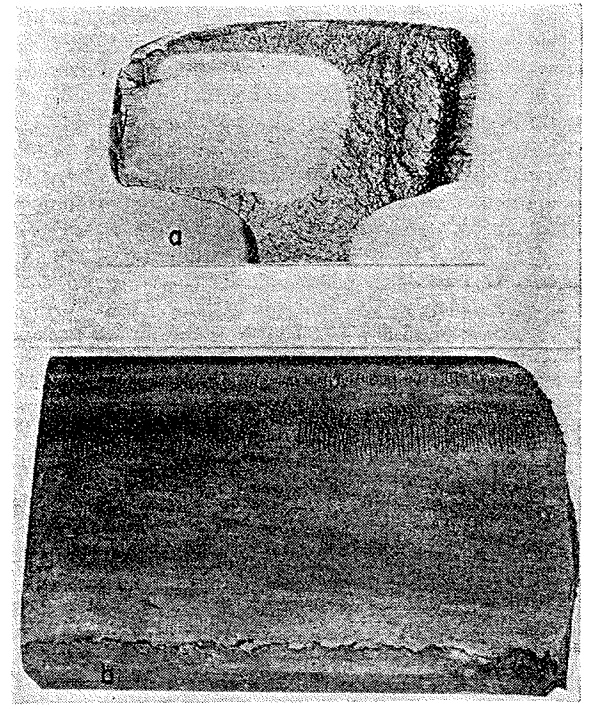


FIG. 18 FATIGUE FAILURE OF RAIL HEAD DUE TO COMBINATION OF NORMAL AND TANGENTIAL LOADING

stresses that occur when the combined normal and tangential forces act on the rail head. After many applications of such combinations of normal and tangential contact loads, cracks in the rail head will form and progress either horizontally or transversely (or both) across the rail head. Figs. 17 and 18 illustrate two of these failures of railway rail probably caused by these stresses.

The theoretical stresses, such as given in this paper, are an important factor in determining the cause of failure, but in actual materials, discontinuities, particularly when they occur at points of high stress, may have a large influence on failure.

Railway Wheels. The foregoing remarks apply also to shelly failures in the rims of wheels used on diesel locomotives. These wheel surfaces are subjected to heavy normal forces due to the weight of the locomotive and to tangential forces due to the driving torque applied through these wheels.

BIBLIOGRAPHY

- 1 "Gesammelte Werke," by H. Hertz, Leipzig, Germany, vol. 1, 1895; English translation in *Miscellaneous Papers*, 1896.
- 2 "Hauptspannungstrajektorie bei der Beruehrung einer Kugel mit einer Platte," by S. Fuchs, *Physikalische Zeitschrift*, vol. 14, 1913, p. 1282.
- 3 "Notes on Hertz's Theory of the Contact of Elastic Bodies," by W. B. Morton and L. J. Close, *Philosophical Magazine*, series 6, vol. 43, 1922, p. 320.
- 4 "Contact Pressures and Stresses," by E. G. Coker and M. S. Ahmed, The Institution of Mechanical Engineers, London, England, vol. 1, July, 1921, p. 365.
- 5 "Stresses Due to the Pressure of One Elastic Solid on Another," by H. R. Thomas and V. A. Hoersch, *Bulletin of Engineering Experiment Station No. 212*, University of Illinois, 1930.
- 6 "Bulletin of Engineers' Ways and Communications," by N. M. Belajef, Leningrad, USSR, 1917; also see "Pitting Due to Rolling Contact," by Stewart Way, *JOURNAL OF APPLIED MECHANICS*, *TRANS. ASME*, vol. 57, 1935, pp. A-49-A-58.
- 7 "Der Spannungszustand und die Austrennung des Werkstoffes bei der Beruehrung Zweier Korper," by L. Foepl, *Forschung auf dem Gebiete des Ingenieurwesens, Ausgabe A*, vol. 7, September-October, 1936, pp. 209-221.
- 8 "Elastische Beruehrung Zweier Halbraeume," by G. Lundberg, *Forschung auf dem Gebiete des Ingenieurwesens, Ausgabe A*, vol. 10, September-October, 1939, pp. 201-211.

- 9 "Compliance of Elastic Bodies in Contact," by R. D. Mindlin, *JOURNAL OF APPLIED MECHANICS*, *TRANS. ASME*, vol. 71, 1949, pp. 259-268.
- 10 "Stresses and Deflections of Cylindrical Bodies in Contact With Application to Contact of Gears and of Locomotive Wheels," by H. Poritsky, *JOURNAL OF APPLIED MECHANICS*, *TRANS. ASME*, vol. 72, 1950, pp. 191-201.
- 11 "Stress and Deformations Due to Tangential and Normal Loads on an Elastic Solid With Applications to Contact Stress," by C. K. Liu, PhD thesis, University of Illinois, June, 1950.
- 12 "The Effect of Range of Stress on the Torsional Fatigue

Strength of Steel," by J. O. Smith, Bulletin No. 316 of Engineering Experiment Station, University of Illinois, 1939.

13 "Stress Distribution and Strength Condition of Two Rolling Cylinders Pressed Together," by E. I. Radzimovsky; Bulletin No. 408, Engineering Experiment Station, University of Illinois, 1953.

14 "The Effect of Range of Stress on the Fatigue Strength of Metals," by J. O. Smith, Bulletin No. 334, Engineering Experiment Station, University of Illinois, 1942.

15 "Fifth Progress Report of the Shelly Rail Studies at the University of Illinois," by R. E. Cramer, Proceedings of the American Railway Engineering Association, vol. 48, 1947, pp. 756-766.

Th
or ro
plete
is an
to be
of an
any)
the d
hand
vecto
phys
meri

Th

$\alpha,$

U

In
consid
oil fil
ing th
damp
which
exam
Inter
cover
is kno
has n
probl

AW
Cor
the A
1952,
Dis
ASME
until
ceives
No
under
of the
Divis